Edelweiss Applied Science and Technology
ISSN: 2576-8484
Vol. 9, No. 9, 1268-1287
2025
Publisher: Learning Gate
DOI: 10.55214/2576-8484.v9i9.10127

From Egyptian stone to sustainable binder: The impact of basalt powder on metakaolin geopolymer cement

Alaa M. Rashad[1,2*], M. H. El-Nashar[3], Fatima Al Zahraa Refaie[1]
[1]Building Materials Research and Quality Control Institute, Housing and Building National Research Center (HBRC), Cairo, Egypt; alaarashad@yahoo.com , rashad@hbrc.edu.eg , a.rashad@su.edu.sa (A.M.R.).
[2]Civil Engineering Department, College of Engineering, Shaqra University, Al-Dawadmi, Riyadh, Saudi Arabia.
[3]Building Physics and Environmental Research Institute, Housing & Building National Research Center (HBRC), Cairo, Egypt.

Abstract: Metakaolin (MK) geopolymers offer a promising avenue for sustainable construction; however, the potential contribution of incorporating natural materials such as basalt powder (BP) remains underexplored. Egypt possesses abundant reserves of both kaolin and basalt, presenting a unique opportunity to develop sustainable construction materials using indigenous resources. This study investigates the feasibility and impact of partially substituting MK with locally sourced BP at incremental levels ranging from 2.5% to 25%. The research aims to comprehensively evaluate the influence of BP integration on specific attributes of MK geopolymer cement. Advanced analytical methods were employed to provide deeper insights into the dataset. The findings indicate that the addition of BP not only improves flowability and shortens setting time but also enhances mechanical strength, reduces drying shrinkage, and improves transport properties. By leveraging indigenous materials and aligning with Egypt's sustainability goals and global carbon reduction efforts, this research contributes to the development of high-performance, resource-efficient geopolymer binders for sustainable construction.

Keywords: *Basalt powder, Drying shrinkage, Fresh and hardened properties, Metakaolin geopolymer, Transport properties.*

1. Introduction

Responding to climate change imperatives and environmental regulations, the construction sector is increasingly adopting sustainable materials, moving away from conventional Portland cement (PC). Cement manufacturing imposes a significant environmental burden, characterized by highly energy-intensive processes that consume nearly 15% of total industrial energy [1]. This heavy energy demand is coupled with a substantial reliance on virgin raw materials, fueling concerns over resource depletion in the coming decades. Additionally, the industry is a recognized source of considerable noise pollution [2]. Cement factories are heavy polluters, releasing massive volumes of greenhouse gases and other air toxins that damage the planet and public health. Key emissions per tonne include ~810 kg of CO_2, heavy metals, 1 kg of SO_2, hydrogen chloride, 2 kg of NOx, and compounds, polychlorinated biphenyls [3] [4]. This substantial environmental footprint makes the industry a major factor in global warming, responsible for roughly 7% of all human-generated CO_2 emissions [5]. Global climate policies targeting 80-90% CO_2 emission reductions by 2050 (from 1990 levels [6]) necessitate major shifts in construction materials. Common mitigation strategies include blending cement with materials like slag [7], silica fume (SF) [8], metakaolin (MK) [9], pumice [10], fly ash (FA) [11]. However, replacing cement with geopolymer binders represents a particularly effective approach to meeting these stringent decarbonization goals.

Geopolymers represent a class of inorganic polymers synthesized through the chemical reaction and subsequent polymerization of aluminosilicate precursors, a process typically initiated by highly alkaline (or sometimes acidic) solutions. The advantages of geopolymers over PC make them a practical replacement option; these include substantially lower energy input [12] and CO_2 generation, remarkable

History: Received: 24 July 2025; Revised: 1 August 2025; Accepted: 6 August 2025; Published: 22 September 2025
* Correspondence: alaarashad@yahoo.com

chemical and thermal durability, advantageous mechanical properties [13], and superior resistance to fire [14]. Commonly, geopolymer synthesis relies on aluminosilicate precursors such as slag [15] MK Rashad [16] and Rashad [17], FA Zhang, et al. [12] and Rashad [18], often supplemented with SF acting as a beneficial additive [19]. The variable nature of slag and FA, stemming from their industrial byproduct origins, complicates their use due to inconsistent chemical/mineral profiles. Coupled with availability limitations relative to the vast scale of cement production, these factors create a clear need and opportunity for MK and other natural materials, such as basalt powder (BP), to be more widely adopted as a geopolymer precursor.MK, derived from the calcination of kaolinite-rich clays, has gained considerable attention due to its high purity, reactivity, and widespread availability Rashad [16] and Jiang, et al. [20]. The geopolymers composed of MK demonstrated satisfactory strength, alongside exceptional durability [21], heightened resistance to heat [22], excellent insulation and electrical properties Bai, et al. [13]; Rashad, et al. [23]; Song, et al. [24] and Rashad [25]. In light of these benefits, scholars have extensively explored ways [26] [27] [28] [29] to enhance the properties of MK through the incorporation of additional natural materials. As illustrated by Nana, et al. [30] the mechanical strength of MK geopolymer was elevated, whilst water absorption decreased when blended with 10-30% volcanic ash. Incorporation of ≤ 30% limestone powder improved MK geopolymer compressive strength [31]. MK geopolymer with natural calcium sources like 10% and 15% CaO or $Ca(OH)_2$ demonstrated a positive influence on compressive strength [32]. Integrating quartz powder, at a maximum of 30%, effectively boosted both workability and compressive strength [33], whilst levels up to 40% increased resilience against harsh marine conditions [34].

Basalt, a widely distributed rock, forms a significant portion of the Earth's crust, accounting for approximately 70% of its composition. It possesses a high silica content [35]. Historically, it has been a staple material for producing tiles. Due to its high abrasion resistance, cast basalt is widely utilized in applications requiring durability, such as street pipe liners in harsh industrial conditions [36]. This versatile rock can be processed into aggregate Boğa and Şenol [37] and Seleem, et al. [38] a binding matrix for PC, or fibers Yang, et al. [39] and Ali, et al. [40]. With its high silica and fitting alumina content, BP shows potential for utilization as a geopolymer precursor, either alone or as part of a blend. Critically, a verification study has confirmed that curing conditions play a major role in the BP geopolymer performance [41]. The sensitivity of geopolymer properties to formulation and processing was further understood by findings related to BP. For instance, both NaOH molarity and applied curing regime pointedly influence pastes combining BP with glass powder. The choice of activator type and its concentration has been proven to pointedly affect the rheology and mechanical performance of 1: 1 BP-slag geopolymer pastes [42]. Additionally, the choice of precursor material is critical, as BP pastes showed lower compressive strength than equal parts BP and slag, as well as 100% slag [43]. High temperatures (up to 900 ℃) severely compromised the compressive strength of alkali-activated slag (AAS) mortars, regardless of whether they contained 20% waster BP [44]. In a recent observation concerning FA geopolymer pastes, incorporating up to 20% BP diminished transport properties while simultaneously improving compressive strength [37].

The integration of natural materials in MK geopolymers presents an opportunity to advance sustainable construction practices, yet the contribution of BP remains underexplored. Egypt, endowed with extensive kaolin reserves across regions like the Sinai Peninsula. Red Sea region, Aswan region (Kalabsha), and the Eastern Desert Rashad [9]; Abdel-Khalek [45] and Rashad [46] is particularly well-suited for the production of MK-based geopolymer cement using indigenous resources. Complementing this kaolin wealth is Egypt's rich basalt deposits, found extensively in the west of Cairo, the neighborhood of the Giza Pyramids [47] Eastern Desert [48] Red Sea Hills Moghazi [49] and Bosworth [50] and volcanic terrains across the nation [51]. Ground basalt yields fine BP with notable pozzolanic properties. Incorporating BP into MK geopolymers offers a compelling pathway to sustainability. Locally sourcing BP reduces dependence on imports, curtails the carbon footprint associated with cement production, and aligns with Egypt's national strategies for sustainable construction, resource efficiency, and industrial carbon emission reduction. Beyond environmental benefits, this approach leverages Egypt's natural

Edelweiss Applied Science and Technology
ISSN: 2576-8484
Vol. 9, No. 9: 1268-1287, 2025
DOI: 10.55214/2576-8484.v9i9.10127

wealth to develop durable, eco-friendly, and high-performance geopolymer-based construction materials, thereby enhancing the technical properties of geopolymers while fostering global material innovation. Driven by the abundant availability of BP and kaolin and guided by Egypt's commitment to sustainable industrial practices, this research explores the feasibility of integrating BP into MK geopolymer cement. It seeks to unlock new potential for Egypt's construction industry and contribute meaningfully to global sustainable construction endeavors. Building on the stated rationale, MK geopolymer was adopted as a reference. Subsequently, MK was partially substituted with BP at incremental levels ranging from 2.5% to 25%. The study aimed to comprehensively assess the influence of BP on flowability, setting time, mechanical performance, transport properties, and drying shrinkage. To ensure robust conclusions, the experimental results were thoroughly analyzed using a suite of scientific.

2. Experimental Details

2.1. Materials

This study primarily utilized powdered kaolin sourced from Egypt's Sinai Peninsula. Kaolinite and quartz are identified as the principal crystalline phases in Figure 1a. The formation of MK was achieved through 2 h calcination process at 750 °C, based on the methodology reported in Rashad [9]; Rashad, et al. [52] and Rashad, et al. [53]. The XRD pattern in Figure 1b reveals that calcination leads to the loss of kaolinite peaks, confirming its transformation into MK, whilst quartz persists as the main crystalline phase. Physical characterization determined the MK powder's specific gravity to be 2.51 and its fineness to be 800 m²/kg. Powdered natural basalt was obtained from a local cement manufacturing facility. The crystalline phases observed in the BP pattern include augite, plagioclase (anorthite/albite), labradorite, and diopside (Figure 2). Physical schematization determined the BP's specific gravity to be 2.8 and its fineness to be 400 m²/kg. Table 1 details the chemical analysis of MK and BP. Compared to MK, BP shows a higher calcium ratio and a lower alumina ratio. However, both materials display relatively similar silica ratios. As seen in Figure 3a, the SEM micrograph reveals that MK particles have irregular shapes, with a subset displaying platy or flaky morphologies. Meanwhile, Figure 3b shows the rough, angular, and highly irregular grains of BP, which is a typical feature of particles derived from the grinding of a hard, crystalline rock, suggesting significant mechanical processing. Both NaOH pellets and sodium silicate were sourced locally, with properties matching those described in [54]. The appearance of each type of powder is generally outlined in Figure 4.

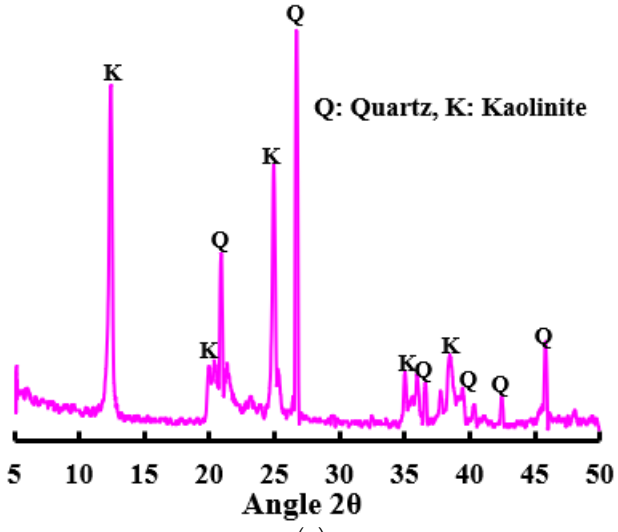

(a)

Edelweiss Applied Science and Technology
ISSN: 2576-8484
Vol. 9, No. 9: 1268-1287, 2025
DOI: 10.55214/2576-8484.v9i9.10127

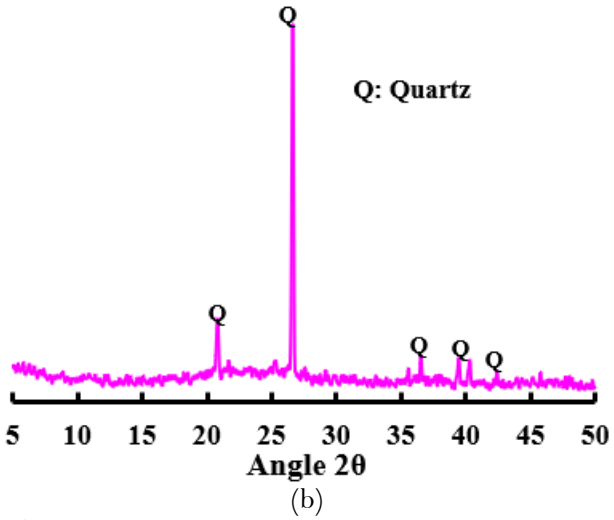

(b)

Figure 1.
XRD pattern of source kaolin (a), and MK (b).

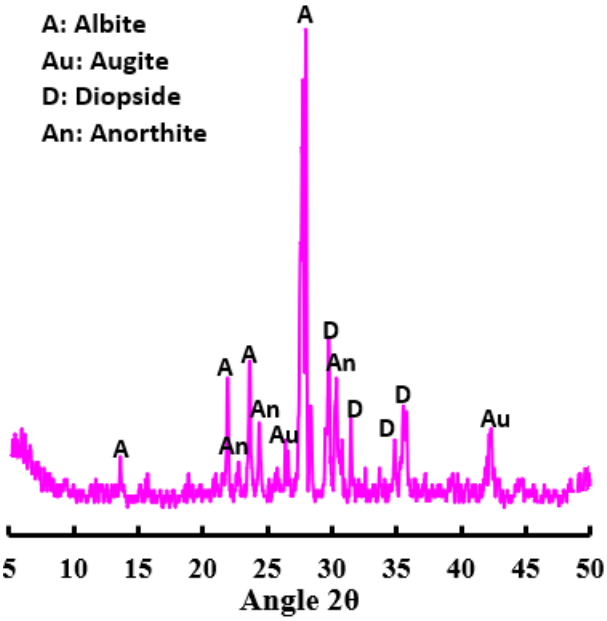

Figure 2.
XRD pattern of BP.

Table 1.
Chemical composition of MK and BP.

Material	Oxide (%)												
	SiO_2	Al_2O_3	Fe_2O_3	CaO	MgO	SO_3	Na_2O	P_2O_5	Cl^-	SrO	K_2O	Other	L.O.I.
MK (%)	52	42	1.49	0.1	0.16	0.15	0.11	0.12	0.04	0	0.12	2.55	1.16
BP (%)	51	15.5	13.3	7.5	4.61	0.14	2.58	0.58	0.01	0.07	1.3	2.39	1.02

Edelweiss Applied Science and Technology
ISSN: 2576-8484
Vol. 9, No. 9: 1268-1287, 2025
DOI: 10.55214/2576-8484.v9i9.10127

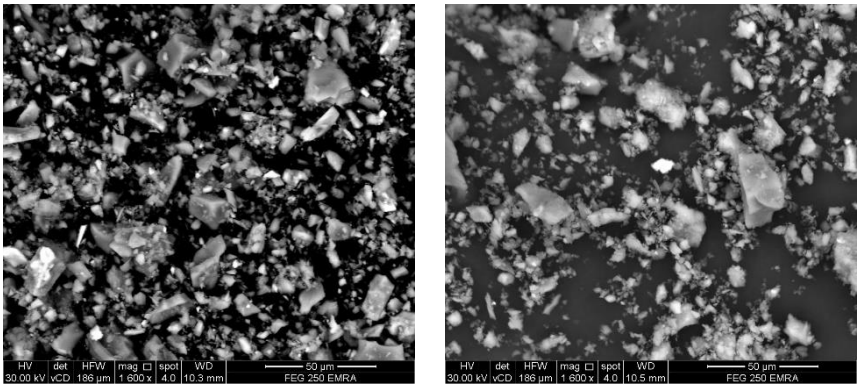

(a) (b)

Figutr 3.
SEM images of MK (a), and BP (b).

(a) MK (b) BP

Figure 4.
Appearance of each type of powder.

2.2. Mix Proportion and Methods

The reference mixture (0BP) consisted entirely of MK, excluding BP. The MK weight was progressively substituted at five different ratios. These ratios included 2.5% (2.5BP), 5% (5BP), 10% (10BP), 15% (15BP), and 25% (25BP). A uniform activator concentration of 40% was maintained throughout the study to examine the influence of varying BP ratios on the characteristics of MK geopolymer cement. The activator solution was made up of 1: 2 combination of NaOH and sodium silicate [55]. A 10 M solution of NaOH was prepared, and this process was initiated at least one day before casting. To guarantee uniform mixing conditions, an additional water/powder ratio of 10% was employed for all mixtures. The details of the mixtures can be found in Table 2.

Table 2.
Mixture details.

ID	0BP	2.5BP	5BP	10BP	15BP	25B
MK	100	97.5	95	90	85	75
PB	0	2.5	5	10	15	25
Extra water/powder	0.1					
Activator/powder	0.4					

The processes of mixing and casting followed the steps detailed in Boğa and Şenol [37]. Each mixture's flow rate and setting time were assessed in line with ASTM C230/C230M-23, and ASTM

Edelweiss Applied Science and Technology
ISSN: 2576-8484
Vol. 9, No. 9: 1268-1287, 2025
DOI: 10.55214/2576-8484.v9i9.10127

C191-08. The initial curing step involved holding the specimens at 80 ℃ for 24 h [56]. After this period, curing conditions diverged depending on specimen type. For the 40 × 40 × 160 mm prisms and 50 mm cubes, the specimens were then kept at room temperature until the testing date. However, the 25 × 25 × 28.5 mm prisms were stored at a controlled environment of 20 ± 1 ℃ and 50% RH, which was employed to measure drying shrinkage as per ASTM C490, and comparable to the apparatus described in Rashad, et al. [52]; Rashad, et al. [53]; Rashad [57] and Rashad, et al. [58]. In short, A bench comparator (0.001 mm precision) was used to measure specimen length variations. Measurements commenced directly after demolding and continued periodically for 56 days. Both flexural and compressive strength tests were conducted at 7, 28, and 56 days. Once the 50 mm cubes had cured for 28 days, their transport properties (ASTM C948-81) were assessed. Flexural tests used 40 × 40 × 160 mm prisms (ASTM C348-21), whilst compressive tests utilized the resulting broken halves from the flexural procedure (ASTM C349:2018). Mirroring the experimental method presented in Rashad and Essa [59] the selected debris samples were characterized using XRD, TGA/DTG, and SEM. Figure 5 provides a schematic of the experimental apparatus.

Edelweiss Applied Science and Technology
ISSN: 2576-8484
Vol. 9, No. 9: 1268-1287, 2025
DOI: 10.55214/2576-8484.v9i9.10127

Figure 5.
A schematic of the experimental apparatus.

3 Results and Discussions

3.1. Flowability

As shown in Figure 6, adjusting BP ratios affects the flowability of the mixtures. Preliminary tests indicate that the 0BP mixture, devoid of BP, has 96 ± 5% flow, surpassing all other mixtures in terms of flow performance. The 0BP's flow represents an improvement over the outcomes in Rashad, et al. [33]; Rashad and Zeedan [60]; El Abd, et al. [61]; Rashad [62] and Rashad and Ouda [63] however, it still lags behind the performance reported in Jaji, et al. [64]; Duan, et al. [65] and Xie, et al. [66] resulting in an intermediate ranking among these cited results. When BP is introduced, a noticeable improvement in flowability is observed. This trend is consistent across the samples, with higher BP ratios leading to progressively greater flow rates. Although the increase is modest at 2.5% BP (from 96 ± 5% to 102 ± 5%), the enhancement becomes significantly more pronounced at 25% BP, where the flow rate rises from 96 ± 5% to 150 ± 5%. The relatively larger particle size of BP, when compared to MK, is likely a contributing factor to this improvement. An additional factor driving this improvement is the angular, somewhat equant shape of the basalt particles. This shape effectively disrupts the inefficient arrangement of the platy metakaolin particles, promoting better particle packing density and reducing friction between particles, thus further enhancing flow. Another important factor is the increased SiO_2/Al_2O_3 ratio with increasing BP ratio [19]. Based on Rashad and Zeedan [60]; Rashad, et al. [67]; Hamdi, et al. [68]; Mahmoodi, et al. [69]; Yaseri, et al. [70]; Khalil, et al. [71] and Rashad, et al. [72] the rheological characteristics of the geopolymer were significantly affected by the SiO_2/Al_2O_3 ratio. Elevating the silica ratio in the blend resulted in enhanced flowability. Notably, Hamdi, et al. [68] established a positive correlation between workability and the SiO_2/Al_2O_3 ratio, observing an improvement as it increased. Similarly, Al-Duais, et al. [73] demonstrated the impact of composition, noting that 100% natural pozzolan mixture showed better flow than one where 20% of the pozzolan was replaced by red mud. It is essential to highlight that incorporating as much as 15% BP into traditional concrete mixtures resulted in a marginal increase in workability [74].

Edelweiss Applied Science and Technology
ISSN: 2576-8484
Vol. 9, No. 9: 1268-1287, 2025
DOI: 10.55214/2576-8484.v9i9.10127

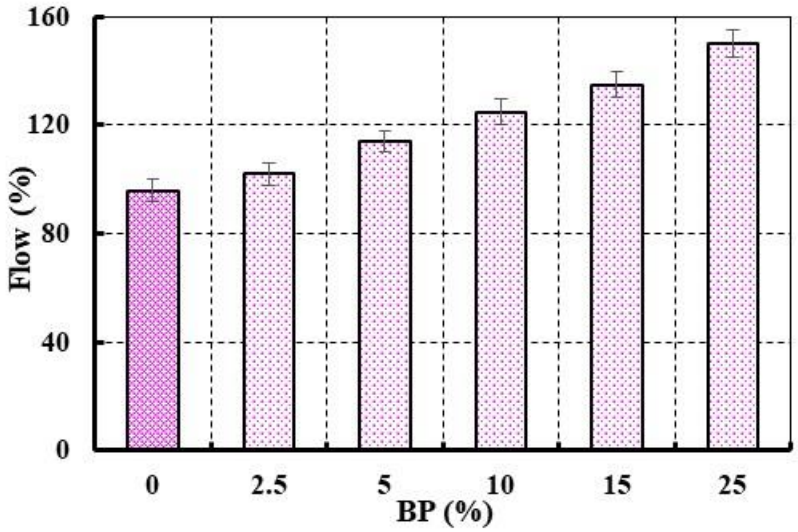

Figure 6.
Flow behavior of mixtures with different BP ratios.

As shown in Figure 7, adjusting BP ratios somewhat affects the setting time of the mixtures. Unsurprising, the BP-free 0BP mixture shows the longest setting time, reflecting the low calcium ratio and slow reactivity of MK [75]. The behavior of the remaining mixtures is governed by their respective BP ratios. In general, setting time appears to decrease slightly with including a lower BP ratio. The initial and final setting times were decreased slightly by 1.85% and 1.77%, respectively, when BP was at its lowest (2.5%). However, at the highest BP ratio (25%), these decreases are 19.2% and 17.2%. These findings could be associated with the higher calcium ratio in BP (7.5%) compared to that in MK (0.1%), since calcium can accelerate the geopolymerization process Rashad [28] and Rashad [29]. The combination of BP and MK introduces a dual source of silica and alumina, promoting greater overall reactivity. The surfaces of the BP particles, along with the localized presence of dissolved calcium ions, act as powerful nucleation sites, promoting the rapid precipitation and growth of the geopolymer gel, much faster than in a pure MK system. Additionally, the calcium ions are not just part of a separate gel phase. Rather, they become chemically embedded within the primary aluminosilicate framework, transforming the binder from a simple N-A-S-H gel into a fast-reaching C-N-A-S-H hybrid gel (see Section 3.6 later). This hybrid structure, with Ca^{2+} ions reinforcing the ionic cross-links, accelerates the precipitation process and leads to a much quicker solidification compared to a pure sodium-based N-A-S-H gel.

Edelweiss Applied Science and Technology
ISSN: 2576-8484
Vol. 9, No. 9: 1268-1287, 2025
DOI: 10.55214/2576-8484.v9i9.10127

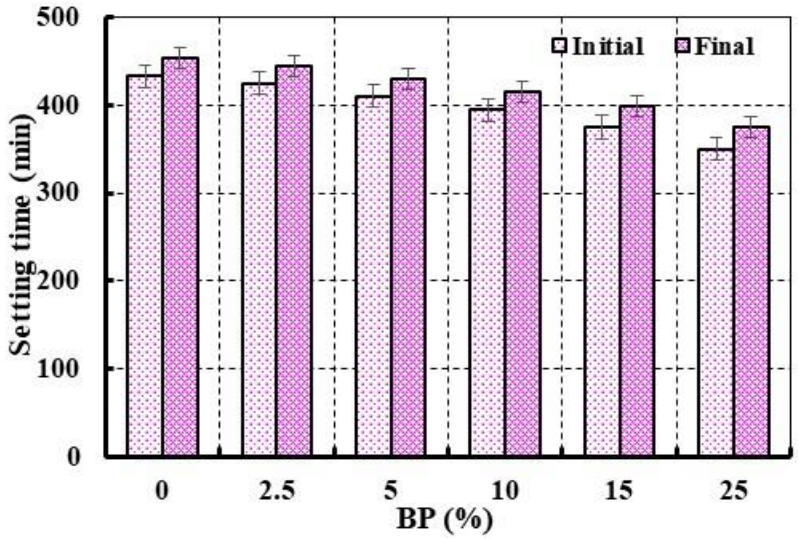

Figure 7.
Setting time behavior of mixtures with different BP ratios.

3.2. Mechanical Strength

As shown in Figure 8, adjusting BP ratios affects the compressive strength of the specimens. Compressive strength is influenced in a patterned way by both curing time and BP ratio. The effect of curing time is consistently positive, leading to enhanced strength. Proper heat curing enables 0BP specimens to develop adequate compressive strength, particularly at an early age. When compared to previous work, the 28 days compressive strength of the mentioned specimens is adhered to the boundaries established in the works cited in Rashad, et al. [33]; Rashad, et al. [34]; Rashad and Ouda [63]; Ruviaro, et al. [76]; Moraes, et al. [77]; Liang, et al. [78]; Ren, et al. [79]; Miao, et al. [80]; Kaya, et al. [81] and Yang, et al. [82]. The behavior of the remaining mixtures is governed by their respective BP ratios. In general, compressive strength appears to increase slightly with including a lower BP ratio. The average compressive strength was increased slightly by 6.64% when BP was at its lowest (2.5%). However, at the highest BP ratio (25%), this increase is 21.61%. Incorporating BP contributes to enhanced strength for several reasons. Although MK is finer in texture, combining it with the coarser particles of BP results in a more optimized particle size distribution. This improved distribution facilitates better particle packing, reducing overall porosity and increasing the final density, and consequently strengthening the material's overall structural integrity. Additionally, raising the BP ratio in the matrix led to a higher SiO_2/Al_2O_3 ratio. Studies confirmed that as the SiO_2/Al_2O_3 ratio rose, up to a specific point, so did the material's compressive strength Rashad [19]; Boğa and Şenol [37]; Rashad and Zeedan [60]; Dehghani, et al. [83]; Lahoti, et al. [84]; Riahi, et al. [85]; Duxson, et al. [86]; Mahfoud, et al. [87] and Marvila, et al. [88]. The higher calcium content in BP compared to MK may contribute to the enhanced strength due to the introduction of calcium into N-A-S-H gel, producing C-N-A-S-H gel (see Section 3.6 later), which is known to form denser, more cross-linked, and less permeable microstructure than pure N-A-S-H gel Ren, et al. [79] and Perez-Cortes and Escalante-Garcia [89]. It has been established that the hybrid C-N-A-S-H gel formed within geopolymer structures plays an essential role in developing compressive strength [90]. The rigid, non-shrinkage BP particles act as internal restraint, physically holding the matrix together and reducing the overall magnitude of shrinkage (see Section 3.4 later). Less shrinkage results in fewer internal defects and a stronger, more durable final product. Fig. 9 provides evidence that adjusting BP ratios affects flexural strength. Incorporating 2.5% BP (2.5BP) results in a marginal increase in flexural strength. As the BP ratio increases, the flexural strength continues to rise, culminating in a peak value of 25% BP. This progression is remarkably similar to the behavior observed for compressive

Edelweiss Applied Science and Technology
ISSN: 2576-8484
Vol. 9, No. 9: 1268-1287, 2025
DOI: 10.55214/2576-8484.v9i9.10127

strength. Other studies Rashad, et al. [52]; Rashad, et al. [58]; Rashad and Abdu [91]; Rashad, et al. [92]; Mohamed, et al. [93]; Zhu, et al. [94]; Kabirova, et al. [95] and Tammam, et al. [96] revealed a like tendency in flexural strength outcomes as was found for compressive strength.

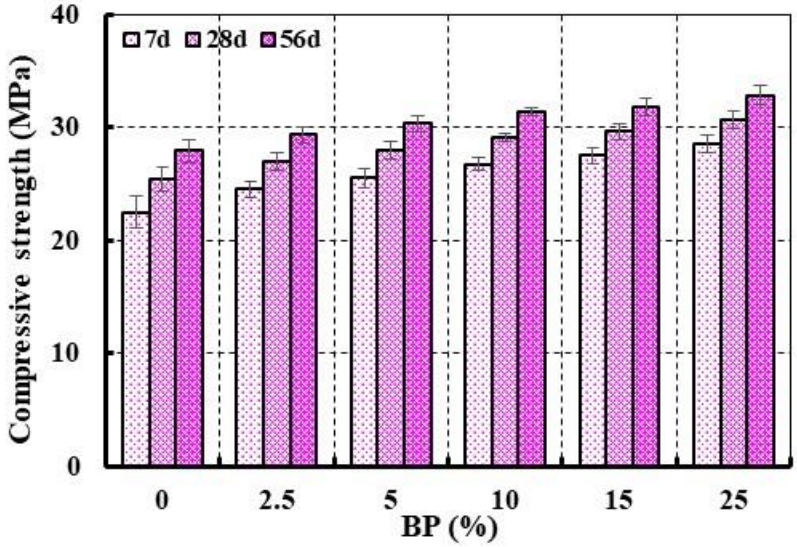

Figure 8.
Compressive strength behavior of specimens with different BP ratios.

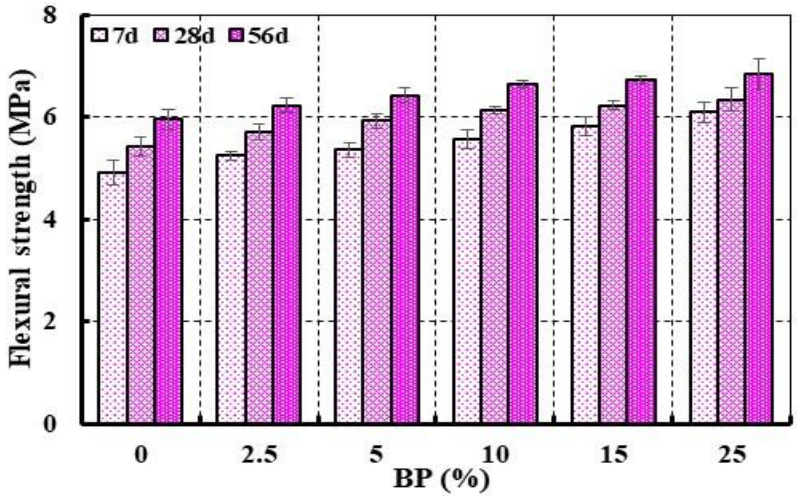

Figure 9.
Flexural strength behavior of specimens with different BP ratios.

3.3. Transport Properties

As shown in Figure 10, adjusting BP ratios affects the transport properties of the specimens. Based on the information, the BP ratio is essential in influencing these properties. The baseline specimens (0BP), devoid of BP, show ~16% water absorption. This result adheres to the boundaries established in the works cited in Bikoko and Bayiha [97]; Borçato, et al. [98]; Djobo and Stephan [99]; Kamseu, et al. [100]. The identical specimens (0BP) exhibit 26% apparent porosity. This finding adheres to the boundaries established in the works cited in Nana, et al. [30]; Eliche-Quesada, et al. [101] and Coelho, et al. [102]. The behavior of the remaining mixtures is governed by their respective BP ratios. In general, transport

Edelweiss Applied Science and Technology
ISSN: 2576-8484
Vol. 9, No. 9: 1268-1287, 2025
DOI: 10.55214/2576-8484.v9i9.10127

properties appear to decrease slightly with including a lower BP ratio. The water absorption decreased slightly from 16% to 15.4%, whilst apparent porosity decreased slightly from 26% to 24.8%, when BP was at its lowest (2.5%). However, at the highest BP ratio (25%), these decreases reach 13.1% (water absorption) and 20.9% (porosity). The factors that contribute to the enhancement of compressive strength, as discussed earlier, also play a key role in reducing transport properties.

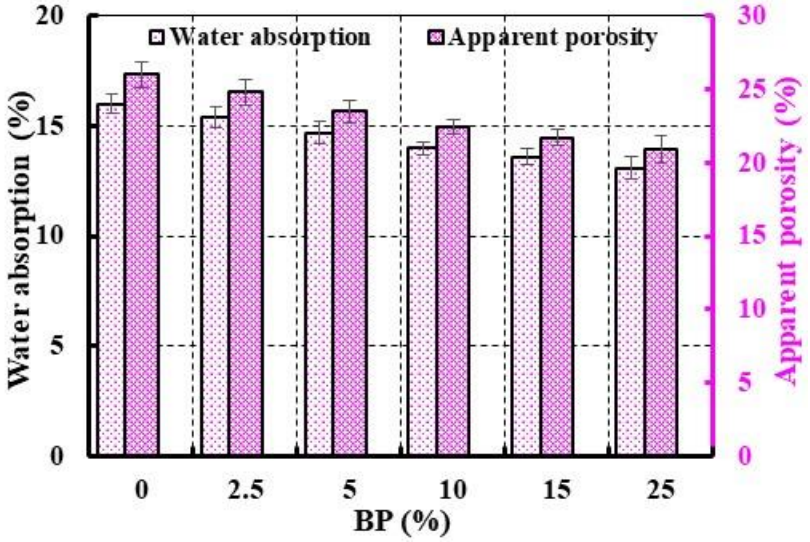

Figure 10.
Transport properties behavior of specimens with different BP ratios.

3.4. Drying Shrinkage

As shown in Figure 11, adjusting BP ratios affects the drying shrinkage of the specimens. The fast reduction of surface moisture in the specimens triggers drying shrinkage, a phenomenon that is most evident during the first few days, a pattern supported by the scientific literature Rashad, et al. [52]; Rashad, et al. [53]; Hasnaoui, et al. [103] and Celerier, et al. [104]. A primary and well-established disadvantage of MK geopolymer is its tendency towards significant drying shrinkage [105]. The highest shrinkage occurs in 0BP specimens, which lack the stabilizing effects of BP. The shrinkage problem is effectively reduced by introducing BP, likely through its role in enhancing the C-N-A-S-H hybrid gel formation. BP's rigid internal skeleton effect creates physical restraint by providing a non-shrinking framework made of larger particles that prevent the fine MK gel from shrinking as it loses water, acting similarly to pebbles in a shrinking sponge. Additionally, by replacing part of the MK with BP, the total volume of the shrinkable geopolymer gel is reduced, thus minimizing shrinkage. BP's coarser particles also reduce the water demand of the mix, leading to less water available for evaporation, which directly decreases the drying shrinkage. These combined benefits make BP a highly effective additive for reducing drying shrinkage in MK-based geopolymers. Thus, with the gradual increase of BP content up to 25%, drying shrinkage progressively declines. Across all specimens, an accelerated shrinkage rate was detected over the initial 16 days, which then transitioned into a slower rate. However, other studies highlighted that this accelerated shrinkage ended within 14 days Huang, et al. [106] and Xu, et al. [107].

Edelweiss Applied Science and Technology
ISSN: 2576-8484
Vol. 9, No. 9: 1268-1287, 2025
DOI: 10.55214/2576-8484.v9i9.10127

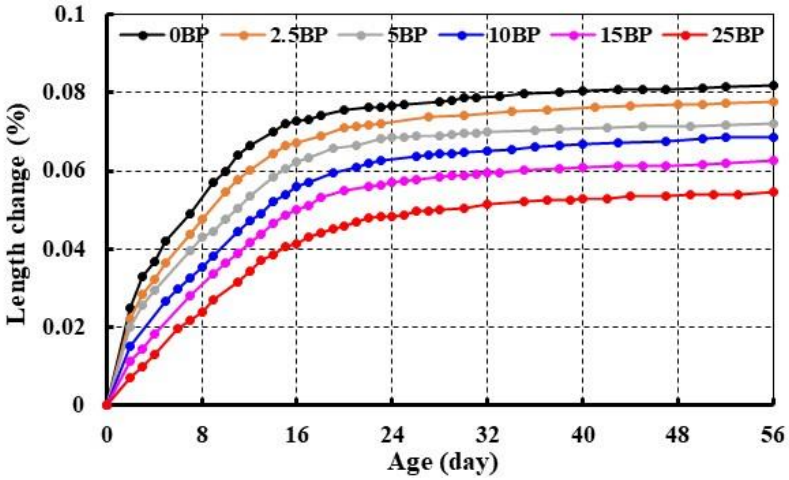

Figure 11.
Drying shrinkage behavior of specimens with different BP ratios.

3.5. Crystalline Phases

Figure 12 provides the XRD patterns for 0BP, 10BP, and 25BP samples. Quartz constitutes the majority of the 0BP sample, which is devoid of BP Rashad, et al. [33]; Rashad, et al. [34]; Rashad, et al. [52] and Rashad and Zeedan [60] while a trace amount of calcite, likely due to carbonation during preparation, can also be detected. The crystalline phase composition of the BP-containing samples (2.5BP, 10BP, and 25BP) is dominated by quartz and albite, with trace levels of calcite, diopside, and augite. A progressive increase in BP content leads to a noticeable enhancement in the albite phase, accompanied by a reduction in quartz content.

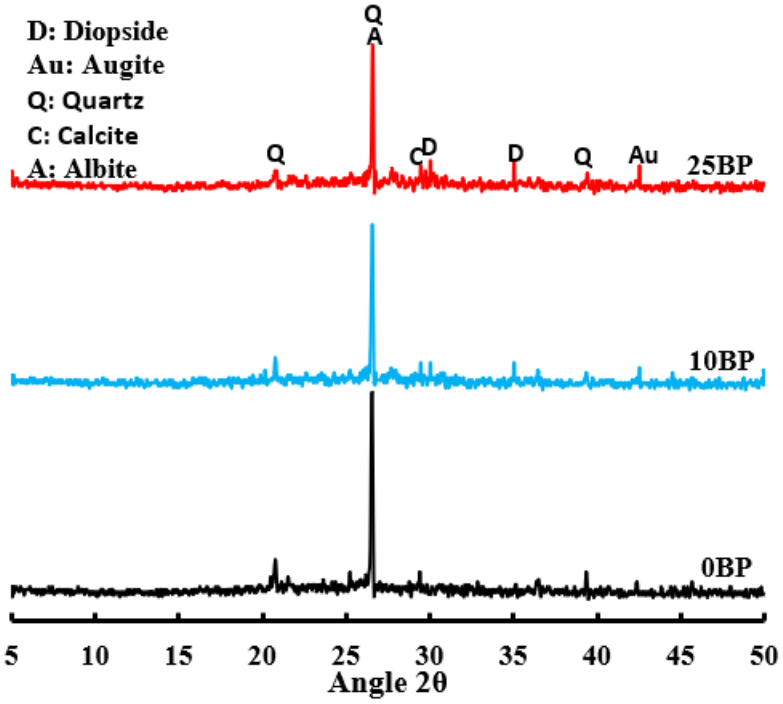

Figure 12.
XRD patterns of 0BP, 10BP, and 25BP samples.

Edelweiss Applied Science and Technology
ISSN: 2576-8484
Vol. 9, No. 9: 1268-1287, 2025
DOI: 10.55214/2576-8484.v9i9.10127

3.6. FTIR Spectrum

Figure 13 provides the FTIR spectra of 0BP, 10BP, and 25BP samples. The 0BP sample shows peaks around ~460 cm^{-1} and 695 cm^{-1} correspond to the bending vibrations of Si-O-Al and Si-O-Si bands, respectively, confirming the formation of aluminosilicate tetrahedral formwork. A band at ~1648 cm^{-1} corresponds to the H-O-H bending (scissoring) vibration. It is a definitive signature of the presence of molecular water within the geopolymer structure, confirming its hydrated nature. A broad and intense band at ~3445 cm^{-1} is associated with O–H stretching vibrations, indicative of hydroxyl functionalities. These arise from physically adsorbed water and from silanol (Si–OH) groups located at the chain ends or defects within the aluminosilicate framework. A dominant band at ~1010 cm^{-1} can be noted, which is due to the asymmetric stretching vibration of Si-O-T bonds (where T is Si or Al). Its position is a characteristic fingerprint of a pure N-A-S-H gel network, the primary binding phase in this sample. A shoulder at ~1400 cm^{-1} indicates the presence of carbonate groups, likely from the reaction of atmospheric CO_2 with the sodium-based activator. The samples containing BP (10BP and 25BP) show similar bands to the control, but the main Si-O-T band has shifted to a lower wavenumber of ~1000 cm^{-1} for the 10BP sample and ~995 cm^{-1} for the 25BP sample. The observed progressive peak shift represents a key finding, providing conclusive evidence that basalt is chemically reactive rather than inert. Calcium ions released from the basalt are actively integrated into the geopolymer network, promoting a transition from a pure N–A–S–H gel to a more complex C–N–A–S–H-type gel. As the basalt content increases, greater calcium incorporation occurs, driving the spectral shift toward regions characteristic of calcium-rich aluminosilicate binders. In cementitious chemistry, C-N-A-S-H gel is known to form a denser, more cross-linked, and less permeable microstructure than pure N-A-S-H gel. This superior microstructure leads to superior mechanical strength.

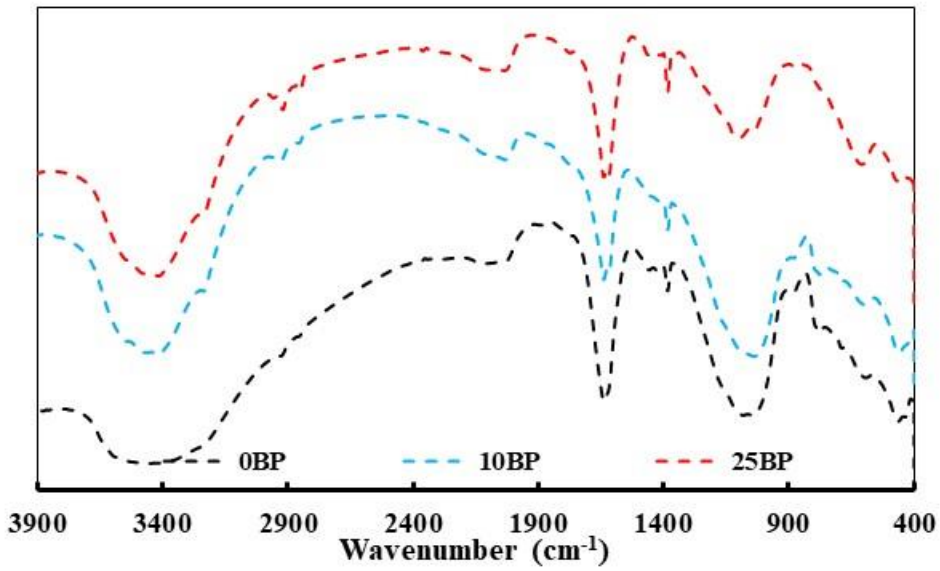

Figure 13.
FTIR spectra of 0BP, 10BP, and 25BP samples.

3.7. Microstructure Analysis

Figure 14 presents SEM micrographs of the 0BP, 10BP, and 25BP samples at varying magnifications. In the absence of BP, the baseline sample (0BP) reveals a heterogeneous structure, marked by a high level of pores and the presence of both undissolved and partially dissolved particles (Fig. 14a). This suggests that some MK particles were either incompletely activated or underwent limited activation during polymerization. The identified features help explain the inferior mechanical performance of the 0BP

Edelweiss Applied Science and Technology
ISSN: 2576-8484
Vol. 9, No. 9: 1268-1287, 2025
DOI: 10.55214/2576-8484.v9i9.10127

specimen in comparison to the others. However, the presence of 10% BP (10BP) results in an obvious change in the microstructure compared to the 0BP sample. The microstructure of the 10BP sample reveals a somewhat homogenous matrix, with fewer pores and undissolved particles (Figure 14b). The improved mechanical strength in 10BP specimens relative to 0BP specimens correlates with the presence of these features. The incorporation of 25% BP (25BP) leads to optimal microstructural enhancement. The 25BP sample exhibits a well-densified structure with improved particle consolidation and a markedly reduced pore count (Fig. 14c), which collectively contribute to its superior mechanical strength compared to other specimens.

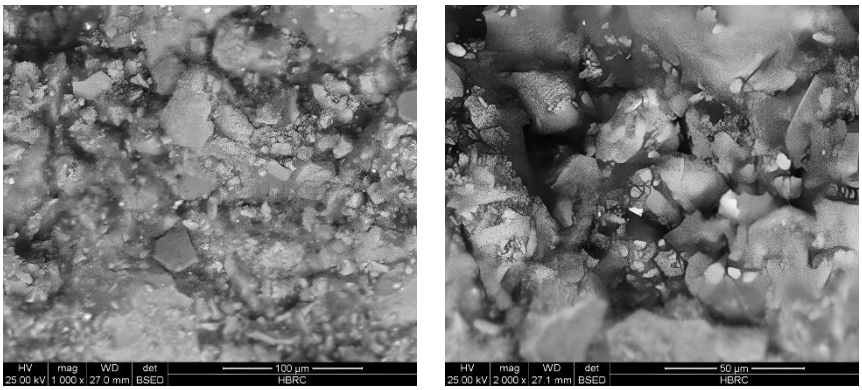

(a) 0BP sample

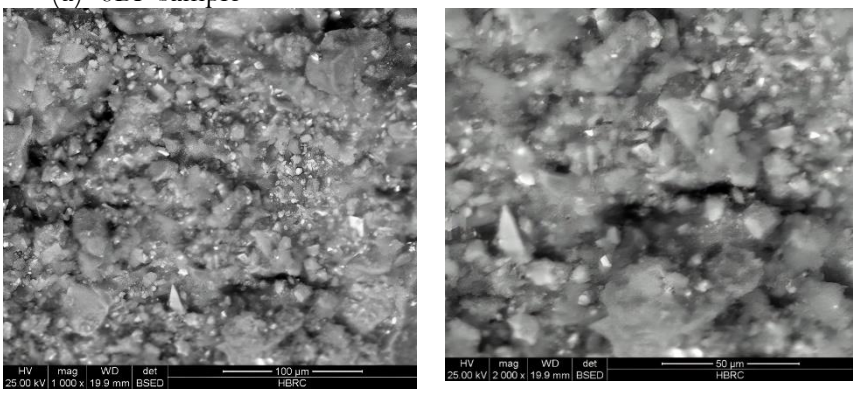

(b) 10BP sample

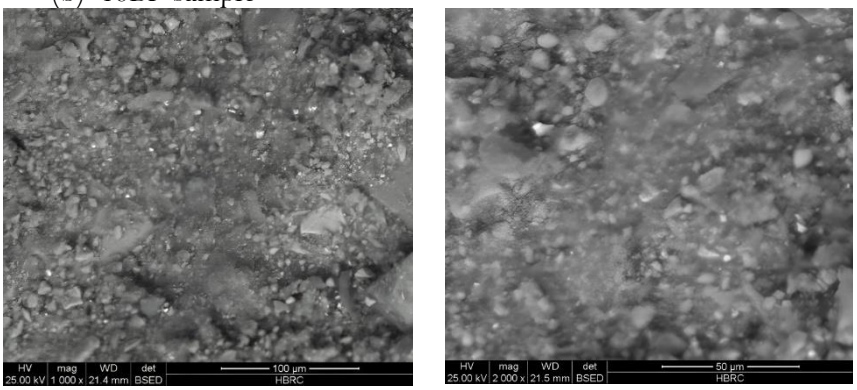

(c) 25BP sample

Figure 14.
SEM images of 0BP, 10BP, and 25 BP samples.

Edelweiss Applied Science and Technology
ISSN: 2576-8484
Vol. 9, No. 9: 1268-1287, 2025
DOI: 10.55214/2576-8484.v9i9.10127

4. Conclusions

Leveraging Egypt's abundant kaolin and basalt reserves, this research successfully investigated the development of a sustainable geopolymer binder through the incorporation of basalt powder into metakaolin. The principal conclusions are:

1. The presence of BP caused an increase in the mixtures' flowability, primarily due to its lower surface area and increased silica ratio.
2. The presence of BP accelerated the setting time, primarily due to the introduction of calcium ions.
3. The mechanical strength increased with higher BP ratios, peaking at 25%. On average, the compressive strength improved by 21.61% at this optimum ratio.
4. The transport properties were progressively reduced as the BP ratio increased up to 25%. At this optimal level, water absorption decreased to 13.1% and apparent porosity to 20.9%, compared to 16% and 26% in specimens without BP, respectively.
5. Drying shrinkage was mitigated with increasing BP content, achieving the most notable reduction at a BP ratio of 25%.
6. The beneficial effect of BP can be attributed to its role in promoting the formation of C-N-A-S-H hybrid gel, increasing the SiO_2/Al_2O_3 ratio, and enhancing the particle size distribution. This optimized distribution improves particle packing, reduces porosity, and increases the final density, all of which contribute to the overall strengthening and improved structural integrity of the material.

Highlights:

BP increased flowability but decreased setting time
BP, up to 25%, increased mechanical strength
BP, up to 25%, decreased transport properties
BP, up to 25%, decreased drying shrinkage

Transparency:

The authors confirm that the manuscript is an honest, accurate, and transparent account of the study; that no vital features of the study have been omitted; and that any discrepancies from the study as planned have been explained. This study followed all ethical practices during writing.

Copyright:

References

[1] A. Mokhtar and M. Nasooti, "A decision support tool for cement industry to select energy efficiency measures," *Energy Strategy Reviews*, vol. 28, p. 100458, 2020.

[2] T. Thai, P. Kučera, and A. Bernatik, "Noise pollution and its correlations with occupational noise-induced hearing loss in cement plants in Vietnam," *International Journal of Environmental Research and Public Health*, vol. 18, no. 8, p. 4229, 2021. https://doi.org/10.3390/ijerph18084229

[3] E. Raffetti, M. Treccani, and F. Donato, "Cement plant emissions and health effects in the general population: a systematic review," *Chemosphere*, vol. 218, pp. 211-222, 2019.

[4] Y. Wu *et al.*, "Geopolymer, green alkali activated cementitious material: Synthesis, applications and challenges," *Construction and Building Materials*, vol. 224, pp. 930-949, 2019. https://doi.org/10.1016/j.conbuildmat.2019.07.112

[5] S. C. Galusnyak, L. Petrescu, and C.-C. Cormos, "Environmental impact assessment of post-combustion CO2 capture technologies applied to cement production plants," *Journal of Environmental Management*, vol. 320, p. 115908, 2022. https://doi.org/10.1016/j.jenvman.2022.115908

[6] L. Meeus, "Appraisal of the European Commission's Energy Roadmap 2050," *European Energy & Climate Journal*, vol. 2, no. 2, pp. 48-56, 2012.

[7] A. M. Rashad, "An overview on rheology, mechanical properties and durability of high-volume slag used as a cement replacement in paste, mortar and concrete," *Construction and Building Materials*, vol. 187, pp. 89-117, 2018.

Edelweiss Applied Science and Technology
ISSN: 2576-8484
Vol. 9, No. 9: 1268-1287, 2025
DOI: 10.55214/2576-8484.v9i9.10127

[8] D. S. Vijayan, P. Devarajan, and A. Sivasuriyan, "A review on eminent application and performance of nano based silica and silica fume in the cement concrete," *Sustainable Energy Technologies and Assessments*, vol. 56, p. 103105, 2023. https://doi.org/10.1016/j.seta.2023.103105
[9] A. M. Rashad, "Metakaolin as cementitious material: History, scours, production and composition–A comprehensive overview," *Construction and building materials*, vol. 41, pp. 303-318, 2013.
[10] A. M. Rashad, "An overview of pumice stone as a cementitious material–the best manual for civil engineer," *Silicon*, vol. 13, no. 2, pp. 551-572, 2021.
[11] A. M. Rashad, "A brief on high-volume Class F fly ash as cement replacement–A guide for Civil Engineer," *International Journal of Sustainable Built Environment*, vol. 4, no. 2, pp. 278-306, 2015.
[12] P. Zhang, Z. Gao, J. Wang, J. Guo, S. Hu, and Y. Ling, "Properties of fresh and hardened fly ash/slag based geopolymer concrete: A review," *Journal of Cleaner Production*, p. 122389, 2020. https://doi.org/10.1016/j.jclepro.2020.122389
[13] C. Bai *et al.*, "A review on metakaolin-based porous geopolymers," *Applied Clay Science*, vol. 258, p. 107490, 2024. https://doi.org/10.1016/j.clay.2024.107490
[14] X. Liu *et al.*, "Investigation on admixtures applied to alkali-activated materials: A review," *Journal of Building Engineering*, vol. 64, p. 105694, 2023. https://doi.org/10.1016/j.jobe.2022.105694
[15] A. M. Rashad, "A comprehensive overview about the influence of different additives on the properties of alkali-activated slag–A guide for Civil Engineer," *Construction and building materials*, vol. 47, pp. 29-55, 2013.
[16] A. M. Rashad, "Alkali-activated metakaolin: A short guide for civil Engineer–An overview," *Construction and Building Materials*, vol. 41, pp. 751-765, 2013.
[17] A. M. Rashad, G. M. F. Essa, E. A. Mossalam, and R. A. Abu-Elwafa, "Enhancing water resistance, improving corrosion behavior, and modifying properties of metakaolin geopolymer cement with trisodium citrate," *Journal of Building Engineering*, vol. 112, 113812, 2025. https://doi.org/10.1016/j.jobe.2025.113812
[18] A. M. Rashad, "A comprehensive overview about the influence of different admixtures and additives on the properties of alkali-activated fly ash," *Materials & Design*, vol. 53, pp. 1005-1025, 2014.
[19] A. M. Rashad, "Silica Fume in Geopolymers: A Comprehensive Review of Its Effects on Properties," *SpringerBriefs in Applied Science and Technology*, 2023. https://doi.org/10.1007/978-3-031-33219-7
[20] T. Jiang, Z. Liu, X. Tian, J. Wu, and L. Wang, "Review on the impact of metakaolin-based geopolymer's reaction chemistry, nanostructure and factors on its properties," *Construction and Building Materials*, vol. 412, p. 134760, 2024. https://doi.org/10.1016/j.conbuildmat.2023.134760
[21] S. A. Bernal and J. L. Provis, "Durability of alkali-activated materials: progress and perspectives," *Journal of the American Ceramic Society*, vol. 97, no. 4, pp. 997-1008, 2014. https://doi.org/10.1111/jace.12831
[22] M. Lahoti, K. H. Tan, and E.-H. Yang, "A critical review of geopolymer properties for structural fire-resistance applications," *Construction and Building Materials*, vol. 221, pp. 514-526, 2019. https://doi.org/10.1016/j.conbuildmat.2019.06.076
[23] A. M. Rashad, O. M. Haraz, A. Elboushi, and W. M. Morsi, "Electrical properties of alkali-activated materials against Portland cement," *Proceedings of the Institution of Civil Engineers-Construction Materials*, vol. 176, no. 1, pp. 33-44, 2023.
[24] Y. Song, C. Xue, W. Guo, Y. Bai, Y. Shi, and Q. Zhao, "Foamed geopolymer insulation materials: Research progress on insulation performance and durability," *Journal of Cleaner Production*, p. 140991, 2024.
[25] A. M. Rashad, "Insulating and fire-resistant behaviour of metakaolin and fly ash geopolymer mortars," *Proceedings of the Institution of Civil Engineers-Construction Materials*, vol. 172, no. 1, pp. 37-44, 2019.
[26] A. M. Rashad, "Effect of nanoparticles on the properties of geopolymer materials," *Magazine of Concrete Research*, vol. 71, no. 24, pp. 1283-1301, 2019.
[27] A. M. Rashad, "Effect of steel fibers on geopolymer properties–The best synopsis for civil engineer," *Construction and Building Materials*, vol. 246, p. 118534, 2020.
[28] A. M. Rashad, "A concise on the effect of calcium oxide on the properties of alkali-activated materials: A manual for civil engineers," *International Journal of Concrete Structures and Materials*, vol. 17, no. 1, p. 72, 2023.
[29] A. M. Rashad, "Calcium hydroxide in geopolymers–a critical overview," *European Journal of Environmental and Civil Engineering*, vol. 29, no. 2, pp. 351-379, 2025.
[30] A. Nana *et al.*, "Mechanical strength and microstructure of metakaolin/volcanic ash-based geopolymer composites reinforced with reactive silica from rice husk ash (RHA)," *Materialia*, vol. 16, p. 101083, 2021.
[31] A. M. Rashad, "Effect of limestone powder on the properties of alkali-activated materials–A critical overview," *Construction and Building Materials*, vol. 356, p. 129188, 2022.
[32] Y. D. Adufu, S. O. Sore, P. Nshimiyimana, A. Messan, and G. Escadeillas, "Effect of calcium-rich additions on the mechanical and microstructural properties of metakaolin-based geopolymer concrete cured in ambient sub-Saharan climate," *Construction and Building Materials*, vol. 453, p. 139009, 2024.
[33] A. M. Rashad, A. A. Hassan, and S. R. Zeedan, "An investigation on alkali-activated Egyptian metakaolin pastes blended with quartz powder subjected to elevated temperatures," *Applied Clay Science*, vol. 132, pp. 366-376, 2016.
[34] A. M. Rashad, A. S. Ouda, and D. M. Sadek, "Behavior of alkali-activated metakaolin pastes blended with quartz powder exposed to seawater attack," *Journal of Materials in Civil Engineering*, vol. 30, no. 8, p. 04018159, 2018.

Edelweiss Applied Science and Technology
ISSN: 2576-8484
Vol. 9, No. 9: 1268-1287, 2025
DOI: 10.55214/2576-8484.v9i9.10127

[35] H. Jamshaid and R. Mishra, "A green material from rock: basalt fiber–a review," *The Journal of The Textile Institute*, vol. 107, no. 7, pp. 923-937, 2016. https://doi.org/10.1080/00405000.2015.1071940

[36] B. Perevozchikova, A. Pisciotta, B. Osovetsky, E. Menshikov, and K. Kazymov, "Quality evaluation of the Kuluevskaya basalt outcrop for the production of mineral fiber, Southern Urals, Russia," *Energy procedia*, vol. 59, pp. 309-314, 2014.

[37] A. R. Boğa and A. F. Şenol, "The effect of waste marble and basalt aggregates on the fresh and hardened properties of high strength self-compacting concrete," *Construction and Building Materials*, vol. 363, p. 129715, 2023. https://doi.org/10.1016/j.conbuildmat.2022.129715

[38] H. E.-D. H. Seleem, A. M. Rashad, and B. A. El-Sabbagh, "Durability and strength evaluation of high-performance concrete in marine structures," *Construction and building Materials*, vol. 24, no. 6, pp. 878-884, 2010.

[39] W. Yang *et al.*, "A review of the mechanical properties and durability of basalt fiber recycled concrete," *Construction and Building Materials*, vol. 412, p. 134882, 2024. https://doi.org/10.1016/j.conbuildmat.2024.134882

[40] A. Ali, R. Hossain, and V. Sahajwalla, "Valorisation of plastic and wood waste through the incorporation in basalt fibre reinforced polymeric composites: A critical review," *Process Safety and Environmental Protection*, p. 107016, 2025. https://doi.org/10.1016/j.psep.2025.107016

[41] R. Gheller, L. L. Silva, M. A. Fiori, and E. R. Batiston, "Exploratory study for the alkaline activation of basalt powder as a supplementary cementitious matrix," *Revista IBRACON de Estruturas e Materiais*, vol. 15, p. e15405, 2022.

[42] B. Akturk, "Fracture behavior of alkali-activated basalt powder/slag systems reinforced with basalt and hybrid fibers," *Materials and Structures*, vol. 56, no. 2, p. 46, 2023.

[43] B. Akturk and B. U. Ayhan, "Alkali-activated basalt powder/slag systems: compressive strength and microstructural characterization," *Materials and Structures*, vol. 56, no. 4, p. 81, 2023.

[44] M. Dener, "Mechanical and durability properties of alkali-activated slag/waste basalt powder mixtures," *Proceedings of the Institution of Mechanical Engineers, Part L: Journal of Materials: Design and Applications*, vol. 237, no. 10, pp. 2250-2265, 2023.

[45] N. A. Abdel-Khalek, "The Egyptian kaolin: An outlook in the view of the new climate of investment," *Applied Clay Science*, vol. 15, no. 3-4, pp. 325-336, 1999.

[46] A. M. Rashad, "Metakaolin effect on geopolymers' properties," *SpringerBriefs in Applied Science and Technology*, 2024. https://doi.org/10.1007/978-3-031-45151-5

[47] A. A. Aal, "Mineral and chemical composition of basalts in the neighbourhood of Giza, Egypt," *Journal of African Earth Sciences*, vol. 26, no. 1, pp. 101-117, 1998.

[48] M. Mostafa, N. Afify, A. Gaber, and E. Abu Zaid, "Investigation of thermal properties of some basalt samples in Egypt," *Journal of Thermal Analysis and Calorimetry*, vol. 75, no. 1, pp. 179-188, 2004.

[49] A.-K. M. Moghazi, "Geochemistry of a Tertiary continental basalt suite, Red Sea coastal plain, Egypt: petrogenesis and characteristics of the mantle source region," *Geological Magazine*, vol. 140, no. 1, pp. 11-24, 2003.

[50] W. Bosworth, "Geological evolution of the Red Sea: historical background, review, and synthesis," *The Red Sea: The formation, morphology, oceanography and environment of a young ocean basin*, pp. 45-78, 2015. https://doi.org/10.1007/978-3-662-45201-1_3

[51] L. M. Mallory-Greenough, J. D. Greenough, and J. V. Owen, "The stone source of Predynastic basalt vessels: Mineralogical evidence for quarries in Northern Egypt," *Journal of Archaeological Science*, vol. 26, no. 10, pp. 1261-1272, 1999.

[52] A. M. Rashad, G. M. Essa, W. Morsi, and E. Fahmy, "Calcium nitrate as a modifier agent for metakaolin-based geopolymer mortar," *Construction and Building Materials*, vol. 456, p. 139199, 2024.

[53] A. M. Rashad, S. R. Zeedan, and M. Gharieb, "Appreciation of sugar beet waste in metakaolin geopolymer mortar for compressive strength and drying shrinkage," *Sustainable Chemistry and Pharmacy*, vol. 37, p. 101429, 2024.

[54] A. M. Rashad, M. F. A. Abdu, and M. Ezzat, "Egyptian volcanic glass powder as a modifier agent for alkali-activated slag cement," *Construction and Building Materials*, vol. 408, p. 133662, 2023.

[55] A. M. Rashad, M. Mokhtar, M. El-Nashar, and R. A.-E. Mohamed, "Waste marble powder emerges as a promising material choice to enhance the properties of alkali-activated slag cement," *Sustainable Chemistry and Pharmacy*, vol. 43, p. 101864, 2025.

[56] A. M. Rashad, Y. A. Mosleh, E. A. Mossalam, and M. Gharieb, "Sodium tripolyphosphate as a modifier agent and a corrosion inhibitor for steel rebar embedded in fly ash geopolymer mortar," *Sustainable Chemistry and Pharmacy*, vol. 41, p. 101721, 2024. https://doi.org/10.1016/j.scp.2024.101721

[57] A. M. Rashad, "Influence of different additives on the properties of sodium sulfate activated slag," *Construction and Building Materials*, vol. 79, pp. 379-389, 2015.

[58] A. M. Rashad, W. Morsi, and S. A. Khafaga, "Effect of limestone powder on mechanical strength, durability and drying shrinkage of alkali-activated slag pastes," *Innovative Infrastructure Solutions*, vol. 6, no. 2, pp. 1-12, 2021.

[59] A. M. Rashad and G. M. Essa, "Effect of ceramic waste powder on alkali-activated slag pastes cured in hot weather after exposure to elevated temperature," *Cement and Concrete Composites*, vol. 111, p. 103617, 2020.

[60] A. M. Rashad and S. R. Zeedan, "Effect of Silica Fume and Activator Concentration on Metakaolin Geopolymer Exposed to Thermal Loads," *ACI Materials Journal*, vol. 120, no. 1, 2023.

Edelweiss Applied Science and Technology
ISSN: 2576-8484
Vol. 9, No. 9: 1268-1287, 2025
DOI: 10.55214/2576-8484.v9i9.10127

[61] A. El Abd *et al.*, "Characteristics and neutron imaging of capillary water absorption for metakaolin and steel fiber reinforced slag based-geopolymer mortars," *Journal of Building Engineering*, vol. 82, p. 107960, 2024.
[62] A. M. Rashad, "Performance of autoclaved alkali-activated metakaolin pastes blended with micro-size particles derivative from dehydroxylation of kaolinite," *Construction and Building Materials*, vol. 248, p. 118671, 2020.
[63] A. M. Rashad and A. S. Ouda, "Thermal resistance of alkali-activated metakaolin pastes containing nano-silica particles," *Journal of Thermal Analysis and Calorimetry*, vol. 136, pp. 609-620, 2019. https://doi.org/10.1007/s10973-018-7657-1
[64] M. B. Jaji, G. P. van Zijl, and A. J. Babafemi, "Slag-modified metakaolin-based 3D printed geopolymer: Mechanical characterisation, microstructural properties, and nitrogen physisorption pore analysis," *Journal of Building Engineering*, vol. 81, p. 108166, 2024.
[65] P. Duan, C. Yan, and W. Luo, "A novel waterproof, fast setting and high early strength repair material derived from metakaolin geopolymer," *Construction and Building Materials*, vol. 124, pp. 69-73, 2016. https://doi.org/10.1016/j.conbuildmat.2016.07.058
[66] X. Xie, T. Liu, J. Zhang, Y. Zheng, and J. Gao, "Effect of acid-activator characteristics on the early hydration behavior and properties of metakaolin-based geopolymer," *Journal of Building Engineering*, vol. 72, p. 106608, 2023.
[67] A. M. Rashad, Y. A. Mosleh, and M. Gharieb, "Preparatory Study about Effect of Feldspar on Properties of Alkali-Activated Slag Concrete," *ACI Materials Journal*, vol. 120, no. 2, 2023.
[68] O. M. Hamdi, A. Ahmed-Chaouch, M. Saïdani, and H. Alioui, "Use of the Algerian natural pozzolan for the production of a geopolymer as a complete cement replacement," *Construction and Building Materials*, vol. 400, p. 132723, 2023. https://doi.org/10.1016/j.conbuildmat.2023.132723
[69] O. Mahmoodi, H. Siad, M. Lachemi, S. Dadsetan, and M. Sahmaran, "Development of ceramic tile waste geopolymer binders based on pre-targeted chemical ratios and ambient curing," *Construction and Building Materials*, vol. 258, p. 120297, 2020.
[70] S. Yaseri, G. Hajiaghaei, F. Mohammadi, M. Mahdikhani, and R. Farokhzad, "The role of synthesis parameters on the workability, setting and strength properties of binary binder based geopolymer paste," *Construction and Building Materials*, vol. 157, pp. 534-545, 2017. https://doi.org/10.1016/j.conbuildmat.2017.09.102
[71] M. G. Khalil, F. Elgabbas, M. S. El-Feky, and H. El-Shafie, "Performance of geopolymer mortar cured under ambient temperature," *Construction and Building Materials*, vol. 242, p. 118090, 2020. https://doi.org/10.1016/j.conbuildmat.2020.118090
[72] A. M. Rashad, A. M. ElNagar, M. El-Nashar, and M. Ezzat, "The use of Egyptian volcanic glass powder as a potential source for improving the properties of alkali-activated fly ash cement," *Sustainable Chemistry and Pharmacy*, vol. 39, p. 101597, 2024. https://doi.org/10.1016/j.scp.2024.101597
[73] I. N. Al-Duais, S. Ahmad, M. M. Al-Osta, M. Maslehuddin, T. A. Saleh, and S. U. Al-Dulaijan, "Optimization of alkali-activated binders using natural minerals and industrial waste materials as precursor materials," *Journal of Building Engineering*, vol. 69, p. 106230, 2023. https://doi.org/10.1016/j.jobe.2023.106230
[74] D. Youness, A. Mechaymech, and R. Al Wardany, "Flow assessment and development towards sustainable self-consolidating concrete using blended basalt and limestone-cement systems," *Journal of Cleaner Production*, vol. 283, p. 124582, 2021.
[75] C. Cui, Y. Dang, C. Luo, L. Wang, and H. Peng, "Mechanical properties and reaction kinetics of alkali-activated metakaolin," *Materials*, vol. 17, no. 2, p. 367, 2024. https://doi.org/10.3390/ma17020367
[76] A. S. Ruviaro *et al.*, "Valorization of oat husk ash in metakaolin-based geopolymer pastes," *Construction and Building Materials*, vol. 367, p. 130341, 2023.
[77] J. Moraes *et al.*, "Influence of sugar cane straw ash in metakaolin-based geopolymers," *Construction and Building Materials*, vol. 444, p. 137835, 2024.
[78] G. Liang, H. Li, H. Zhu, T. Liu, Q. Chen, and H. Guo, "Reuse of waste glass powder in alkali-activated metakaolin/fly ash pastes: Physical properties, reaction kinetics and microstructure," *Resources, Conservation and Recycling*, vol. 173, p. 105721, 2021. https://doi.org/10.1016/j.resconrec.2021.105721
[79] J. Ren, B. C. Acarturk, N. D. Dowdy, and W. V. Srubar III, "The effects of calcium carbonate on sodium metasilicate-activated metakaolin-based geopolymer pastes," *Construction and Building Materials*, vol. 448, p. 138218, 2024.
[80] X. Miao, X. Pang, S. Li, H. Wei, J. Yin, and X. Kong, "Mechanical strength and the degradation mechanism of metakaolin based geopolymer mixed with ordinary Portland cement and cured at high temperature and high relative humidity," *Chinese Journal of Chemical Engineering*, 2023.
[81] M. Kaya, F. Köksal, M. Bayram, M. Nodehi, O. Gencel, and T. Ozbakkaloglu, "The effect of marble powder on physico-mechanical and microstructural properties of kaolin-based geopolymer pastes," *Structural Concrete*, vol. 24, no. 5, pp. 6485-6504, 2023. https://doi.org/10.1002/suco.202201010
[82] T. Yang, H. Zhu, and Z. Zhang, "Influence of fly ash on the pore structure and shrinkage characteristics of metakaolin-based geopolymer pastes and mortars," *Construction and Building Materials*, vol. 153, pp. 284-293, 2017.
[83] A. Dehghani, F. Aslani, and N. G. Panah, "Effects of initial SiO2/Al2O3 molar ratio and slag on fly ash-based ambient cured geopolymer properties," *Construction and Building Materials*, vol. 293, p. 123527, 2021. https://doi.org/10.1016/j.conbuildmat.2021.123527

Edelweiss Applied Science and Technology
ISSN: 2576-8484
Vol. 9, No. 9: 1268-1287, 2025
DOI: 10.55214/2576-8484.v9i9.10127

[84] M. Lahoti, P. Narang, K. H. Tan, and E.-H. Yang, "Mix design factors and strength prediction of metakaolin-based geopolymer," *Ceramics International*, vol. 43, no. 14, pp. 11433-11441, 2017. https://doi.org/10.1016/j.ceramint.2017.06.006

[85] S. Riahi, A. Nemati, A. Khodabandeh, and S. Baghshahi, "The effect of mixing molar ratios and sand particles on microstructure and mechanical properties of metakaolin-based geopolymers," *Materials Chemistry and Physics*, vol. 240, p. 122223, 2020.

[86] P. Duxson, S. W. Mallicoat, G. C. Lukey, W. M. Kriven, and J. S. Van Deventer, "The effect of alkali and Si/Al ratio on the development of mechanical properties of metakaolin-based geopolymers," *Colloids and Surfaces A: Physicochemical and Engineering Aspects*, vol. 292, no. 1, pp. 8-20, 2007. https://doi.org/10.1016/j.colsurfa.2006.05.044

[87] E. Mahfoud, K. Ndiaye, W. Maherzi, S. Aggoun, M. Benzerzour, and N.-E. Abriak, "Mechanical properties and shrinkage performance of one-part-geopolymer based on fly ash and micronized dredged sediments," *Developments in the Built Environment*, vol. 16, p. 100253, 2023.

[88] M. T. Marvila, A. R. Azevedo, G. C. Delaqua, B. C. Mendes, L. G. Pedroti, and C. M. Vieira, "Performance of geopolymer tiles in high temperature and saturation conditions," *Construction and Building Materials*, vol. 286, p. 122994, 2021.

[89] P. Perez-Cortes and J. I. Escalante-Garcia, "Gel composition and molecular structure of alkali-activated metakaolin-limestone cements," *Cement and Concrete Research*, vol. 137, p. 106211, 2020.

[90] D. Das and P. K. Rout, "Synthesis and characterization of fly ash and GBFS based geopolymer material," *Biointerface Res Appl Chem*, vol. 11, pp. 14506-14519, 2021. https://doi.org/10.33263/BRIAC116.14506514519

[91] A. M. Rashad and M. F. A. Abdu, "Accelerated aging resistance, abrasion resistance and other properties of alkali-activated slag mortars containing limestone powder," *Sustainable Chemistry and Pharmacy*, vol. 37, p. 101406, 2024.

[92] A. M. Rashad, H. Mohamed, M. H. Khalil, H. Hammed, and A. El-Gamal, "Effect of micro-sized lead oxide on the workability, mechanical strength and durability of alkali-activated slag mortar," *Construction and Building Materials*, vol. 373, p. 130890, 2023.

[93] H. Mohamed, A. El-Gamal, M. H. Khalil, H. Hammed, and A. M. Rashad, "Valorization of nano-PbO as an additive to modify the properties and radiation shielding of alkali-activated slag mortar," *Materials Chemistry and Physics*, vol. 287, p. 126277, 2022.

[94] X. Zhu, X. Kang, J. Deng, K. Yang, S. Jiang, and C. Yang, "Chemical and physical effects of high-volume limestone powder on sodium silicate-activated slag cement (AASC)," *Construction and Building Materials*, vol. 292, p. 123257, 2021. https://doi.org/10.1016/j.conbuildmat.2021.123257

[95] A. Kabirova *et al.*, "Physical and mechanical properties of metakaolin-based geopolymer mortars containing various waste powders," *European Journal of Environmental and Civil Engineering*, vol. 27, no. 1, pp. 437-456, 2023. https://doi.org/10.1080/19648189.2022.2050303

[96] Y. Tammam, M. Uysal, and O. Canpolat, "Effects of alternative ecological fillers on the mechanical, durability, and microstructure of fly ash-based geopolymer mortar," *European Journal of Environmental and Civil Engineering*, pp. 1-24, 2021.

[97] T. G. L. Bikoko and B. N. Bayiha, "Effects of marble addition on the fresh, physical, mechanical, and optical microscopic properties of metakaolin-based geopolymer binders," *Innovative Infrastructure Solutions*, vol. 8, no. 1, p. 3, 2023. https://doi.org/10.1007/s41062-022-00960-3

[98] A. G. Borçato, M. Thiesen, and R. A. Medeiros-Junior, "Incorporation of clay brick wastes and calcium hydroxide into geopolymers: Compressive strength, microstructure, and efflorescence," *Journal of Building Engineering*, vol. 88, p. 109259, 2024. https://doi.org/10.1016/j.jobe.2024.109259

[99] J. N. Y. Djobo and D. Stephan, "The reaction of calcium during the formation of metakaolin phosphate geopolymer binder," *Cement and Concrete Research*, vol. 158, p. 106840, 2022. https://doi.org/10.1016/j.cemconres.2022.106840

[100] E. Kamseu *et al.*, "Substitution of sodium silicate with rice husk ash-NaOH solution in metakaolin based geopolymer cement concerning reduction in global warming," *Journal of cleaner production*, vol. 142, pp. 3050-3060, 2017. https://doi.org/10.1016/j.jclepro.2016.10.164

[101] D. Eliche-Quesada, A. Calero-Rodríguez, E. Bonet-Martínez, L. Pérez-Villarejo, and P. J. Sánchez-Soto, "Geopolymers made from metakaolin sources, partially replaced by Spanish clays and biomass bottom ash," *Journal of Building Engineering*, vol. 40, p. 102761, 2021. https://doi.org/10.1016/j.jobe.2021.102761

[102] T. Coelho, B. Bezerra, J. Verza, A. Luz, and M. Morelli, "Physico-mechanical properties of metakaolin and diatomite-based geopolymers," *Materials Letters*, vol. 349, p. 134784, 2023. https://doi.org/10.1016/j.matlet.2023.134784

[103] A. Hasnaoui, A. Bourguiba, N. Sebaibi, and M. Boutouil, "Valorization of queen scallop shells in the preparation of metakaolin-based geopolymer mortars," *Journal of Building Engineering*, vol. 53, p. 104578, 2022. https://doi.org/10.1016/j.jobe.2022.104578

[104] H. Celerier, J. Jouin, N. Tessier-Doyen, and S. Rossignol, "Influence of various metakaolin raw materials on the water and fire resistance of geopolymers prepared in phosphoric acid," *Journal of Non-Crystalline Solids*, vol. 500, pp. 493-501, 2018. https://doi.org/10.1016/j.jnoncrysol.2018.09.005

[105] M. Mastali, P. Kinnunen, A. Dalvand, R. M. Firouz, and M. Illikainen, "Drying shrinkage in alkali-activated binders–a critical review," *Construction and Building Materials*, vol. 190, pp. 533-550, 2018.

Edelweiss Applied Science and Technology
ISSN: 2576-8484
Vol. 9, No. 9: 1268-1287, 2025
DOI: 10.55214/2576-8484.v9i9.10127

[106] D. Huang, P. Chen, H. Peng, Q. Yuan, and X. Tian, "Drying shrinkage performance of Medium-Ca alkali-activated fly ash and slag pastes," *Cement and Concrete Composites*, vol. 130, p. 104536, 2022.
[107] R. Xu, F. Kong, R. Yang, H. Wang, and T. Hong, "Drying shrinkage mitigation of alkali-activated blast furnace slag-copper slag by polyether-based shrinkage reducing admixture and MgO-based expansion agent," *Construction and Building Materials*, vol. 416, p. 135172, 2024.

Edelweiss Applied Science and Technology
ISSN: 2576-8484
Vol. 9, No. 9: 1268-1287, 2025
***DOI:** 10.55214/2576-8484.v9i9.10127*